Role of Antisymmetric Exchange in Selecting Magnetic Chirality in $Ba_3NbFe_3Si_2O_{14}$

A. Zorko,[1,2] M. Pregelj,[1] A. Potočnik,[1] J. van Tol,[3] A. Ozarowski,[3] V. Simonet,[4] P. Lejay,[4] S. Petit,[5] and R. Ballou[4]

[1]*Jožef Stefan Institute, Jamova 39, SI-1000 Ljubljana, Slovenia*
[2]*EN-FIST Centre of Excellence, Dunajska 156, SI-1000 Ljubljana, Slovenia*
[3]*National High Magnetic Field Laboratory, Florida State University, Tallahassee, Florida 32310*
[4]*Institut Néel, CNRS and Université Joseph Fourier, BP 166, 38042 Grenoble, France*
[5]*Laboratoire Léon Brillouin, CEA-CNRS, CE-Sacley, F-91191 Gif sur Yvette, France*

(Received 5 August 2011; published 16 December 2011)

We present an electron spin resonance (ESR) investigation of the acentric $Ba_3NbFe_3Si_2O_{14}$, featuring a unique single-domain double-chiral magnetic ground state. Combining simulations of the ESR linewidth anisotropy and the antiferromagnetic-resonance modes allows us to single out the Dzyaloshinsky-Moriya (DM) interaction as the leading magnetic anisotropy term. We demonstrate that the rather minute out-of-plane DM component $d_c = 45$ mK is responsible for selecting a unique ground state, which endures thermal fluctuations up to astonishingly high temperatures.

DOI: 10.1103/PhysRevLett.107.257203 PACS numbers: 75.30.Gw, 76.30.−v, 76.50.+g

Spin-orbit coupling generally has no relevant effect in ordinary magnets, except to pin the orientation of spins with respect to the background lattice in magnetically ordered phases, singled out by the isotropic Heisenberg exchange interactions. An exception is provided on geometrically frustrated lattices where the isotropic interactions alone are often unable to raise the macroscopic degeneracy of a ground state (GS) [1], leading to unconventional cooperative electronic states [1–4]. Then, the magnetic behavior might be exclusively driven by minute perturbing terms in the form of anisotropic interactions emanating from the spin-orbit coupling. For instance, the antisymmetric Dzyaloshinsky-Moriya (DM) exchange interaction [5] can induce order on a kagome lattice in the classical limit [6–8] and can lead to quantum criticality in the quantum limit [9]. Furthermore, DM exchange interaction is known to alter phase diagrams of frustrated ladders [10] and triangular lattices [11]. It is also responsible for spin chirality [12] that can be long-ranged even in the absence of a classical magnetic order [13]. Spin chirality is one of the key concepts in the physics of strongly correlated electrons, as it is related to various intriguing phenomena, like the realization of spin liquids [14], magnetic-order induced ferroelectricity [15], anomalous Hall effect [16], and possibly high-temperature superconductivity [17].

In this context, $Ba_3NbFe_3Si_2O_{14}$ (BNFSO) is extremely appealing due to its remarkable magnetic properties. It crystallizes in a noncentrosymmetric trigonal unit cell (P321 symmetry). The Fe^{3+} ($S = 5/2$) spins reside on vertices of equilateral triangles arranged into a two-dimensional (2D) triangular lattice (crystallographic ab planes in Fig. 1) [18]. The dominant exchange interactions are antiferromagnetic—the Curie-Weiss temperature is $\theta \sim -180$ K [18–20]—and thus frustrated. Nevertheless, a long-range-ordered (LRO) state is realized below $T_N = 26$ K, characterized by a 120° spin arrangement on each triangle. The moments are bound to the ab planes and form a magnetic helix along the crystallographic c axis, corresponding to the magnetic propagation vector $\mathbf{q} = (0, 0, \tau)$, $\tau \sim 1/7$ [18].

The system has been drawing considerable attention because of its magnetoelectric and multiferroic properties [19–21]. However, its uniqueness stems from its distinctive magnetic order and magnetic excitations. The LRO magnetic GS is doubly chiral [Fig. 1(b)] and single-domain—a single triangular vector chirality ϵ_Δ together with a single helicity ϵ_H is chosen from four possible states in a structurally chiral crystal—which is believed to be crucial for its multiferroic properties [18]. Moreover, below T_N one of the two magnetic excitation branches emerging from the magnetic satellites is completely chiral over the whole energy spectrum, implying an unprecedented absence of

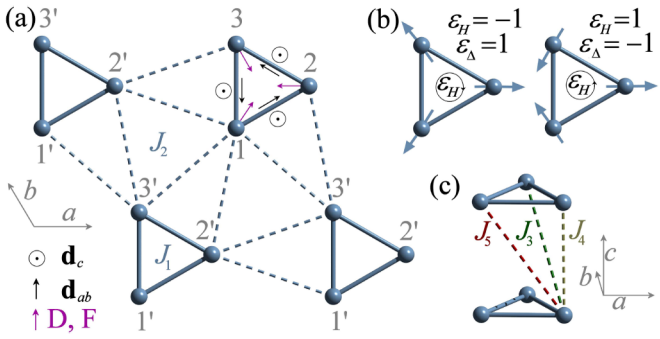

FIG. 1 (color online). 2D "triangular" arrangement of Fe^{3+} in BNFSO. (a),(c) Exchange interactions J_{1-5} and magnetic anisotropies of the Dzyaloshinsky-Moriya (**d**) and single-ion (**D**, **F**) type. The latter vectors are parallel to a local twofold rotational axis defining the Z axis. (b) Two possible double chiral ground states, with ϵ_Δ and ϵ_H denoting triangular chirality and helicity (with $\sim 2\pi/7$ pitch along c axis), respectively.

 © 2011 American Physical Society

chirality mixing of the spin dynamics [22]. The chiral correlations remain present far above T_N [23]. The helicity of the GS can be rationalized within the isotropic Heisenberg model if three competing interplane interactions [J_{3-5} in Fig. 1(c)] are considered. However, the isotropic exchange still allows [18] for two (ϵ_H, ϵ_Δ) pairs [Fig. 1(b)], and fails to justify the selection of the ab easy plane. Thus, the fundamental question about the mechanism, responsible for the experimentally observed unique single-domain chiral GS [18] in BNFSO, arises.

It was suggested that the DM anisotropy might be responsible for selecting the chiral GS [18] and for opening a small gap in magnetic excitations [22] of BNFSO. In another inelastic neutron scattering (INS) study the latter was proposed to arise from single-ion (SI) anisotropy [23]. A clear and quantitative determination of the source of the magnetic anisotropy and of its impact on the GS is therefore needed. In this Letter, we present our electron spin resonance (ESR) study, which provides a direct insight into the magnetic anisotropy of BNFSO. Jointly simulating the experimental ESR linewidth anisotropy in the paramagnetic phase and magnetic excitations in the ordered phase, we determine the dominant magnetic anisotropy, which is of the DM type and has both a sizable out-of-plane (d_c) and in-plane (d_{ab}) component (Fig. 1). Our mean-field based calculations single out d_c as being responsible for selecting the unique GS.

ESR is an extremely powerful technique for quantifying magnetic anisotropy [24]. The isotropic Heisenberg exchange commutes with the S_z spin operator (z denotes the quantization axis set by the applied magnetic field) and therefore leads to a δ-function resonance. Finite magnetic anisotropy then yields a finite ESR linewidth. In single crystals the linewidth anisotropy in the paramagnetic phase can often unveil the dominant magnetic anisotropy, since different types of anisotropy reflect local symmetries distinctively, as they arise from different microscopic origins. Finally, ESR can also detect collective magnon modes in a LRO state. We therefore performed an extensive ESR investigation on high-quality BNFSO single crystals in the temperature range between 4 K and 500 K. X-band (at 9.3 GHz) spectra were recorded on a homemade double-cavity spectrometer, equipped with a helium-flow cooling and a preheated-nitrogen-flow heating system. Measurements at frequencies between 50 GHz and 400 GHz were performed on a couple of custom-made transmission-type spectrometers at the National High Magnetic Field Laboratory, Florida.

In the X band, Lorentzian-shaped spectra are observed down to T_N (Fig. 2), in accord with strong exchange narrowing regularly encountered in dense magnetic systems. Below T_N, the paramagnetic signal rapidly disappears. Our calibration of the ESR intensity, which is proportional to spin-only magnetic susceptibility χ_{ESR}, and the scaling between χ_{ESR} and the bulk susceptibility

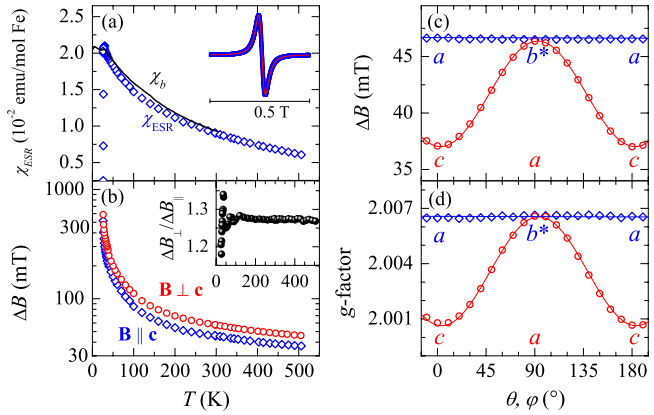

FIG. 2 (color online). X-band ESR results: (a) Comparison of ESR, χ_{ESR}, and bulk, χ_b, susceptibility for $\mathbf{B}\|\mathbf{c}$. Inset: room-temperature ESR spectrum (blue [dark gray]) and the corresponding Lorentzian fit (red [medium gray]). (b) Temperature dependence of linewidths and the linewidth ratio (inset). Angular dependence of (c) the linewidth and (d) the g factor measured at 500 K, with corresponding fits (solid lines) explained in the text.

χ_b [Fig. 2(b)] prove that the ESR signal of BNFSO is intrinsic. The observed small deviations of the g factor from the free-electron value $g_0 = 2.0023$ are typical for Fe^{3+} with a nearly pure ${}^6S_{5/2}$ orbital singlet GS [24]. A uniaxial anisotropy of the g tensor and the linewidth [Figs. 2(c) and 2(d)] is justified by a threefold rotational symmetry of iron triangles. Our fit of the g-factor anisotropy [25] yields the three eigenvalues of the g tensor: $g_{XX} = 2.000$, $g_{YY} = 2.001$, and $g_{ZZ} = 2.013$, and thus reveals that also locally the symmetry of the g tensor is very close to being uniaxial. The polar axis Z on each site is set by a local twofold rotational axis lying within the crystallographic ab plane (a direction for site 2 in Fig. 1). The other two principal axes X and Y for site 2 lie 30° and 120° from the b^* axis in the crystallographic b^*c plane [25].

The anisotropy of the g factor reflects mixing of excited orbital states into the ground orbital singlet of the Fe^{3+} ion, which is induced by a spin-orbit coupling. The anisotropy of the linewidth arises from magnetic anisotropy present in a spin Hamiltonian, which originates from the same perturbation. We address the issue of the magnetic anisotropy in BNFSO in the framework of the spin Hamiltonian

$$\mathcal{H} = \sum_{(ij)} J_{ij}\mathbf{S}_i \cdot \mathbf{S}_j - \mu_B \mathbf{B} \cdot \mathbf{g} \cdot \sum_j \mathbf{S}_j + \mathcal{H}', \qquad (1)$$

where, the first sum runs oven the spin pairs connected by one of the five different exchange interactions (Fig. 1) and represents the Heisenberg term $\mathcal{H}_e$, the second sum gives the Zeeman coupling $\mathcal{H}_Z$ and the third term the magnetic anisotropy $\mathcal{H}'$. The two dominant contributions [26] to the latter for Fe^{3+} are the single-ion anisotropy [24]

$$\mathcal{H}'_{\mathrm{SI}} = \sum_j \Big[D S^2_{j,Z} + \frac{a}{6}(S^4_{j,X} + S^4_{j,Y} + S^4_{j,Z}) + \frac{F}{180}\Big(35 S^4_{j,Z} - \frac{475}{2} S^2_{j,Z}\Big)\Big] + \text{const}, \quad (2)$$

and the Dzyaloshinsky-Moriya anisotropy [5]

$$\mathcal{H}'_{\mathrm{DM}} = \sum_{(ij)} \mathbf{d}_{ij} \cdot \mathbf{S}_i \times \mathbf{S}_j. \quad (3)$$

The symmetry of the SI anisotropy is the same as that of the g tensor [27]; therefore, we omit the additional $E(S^2_X - S^2_Y)$ term. Since J_1 is dominant [22,23], we consider the DM interaction only between nearest neighbors. The DM vector may possess a nonzero out-of-plane d_c and in-plane d_{ab} component parallel to the bond [Fig. 1(a)]. The third component is forbidden by the twofold rotational axis passing through the middle of each bond.

Using the Kubo-Tomita approach [28], we can analytically calculate the linewidth anisotropy $\Delta B_\infty(\theta)$ at infinite temperature, separately for both types of magnetic anisotropy [25]. At finite temperatures $\Delta B(\theta) = c(\theta, T)\Delta B_\infty(\theta)$, where $c(\theta, T)$ differs from unity due to finite spin correlations. In BNFSO the uncorrelated paramagnetic state is not reached yet even at 500 K ($\sim 3\theta$) [Fig. 2(b)], which complements specific heat measurements showing that 20% of magnetic entropy is still missing at 200 K [20]. This needs to be contrasted with several Cu-based 2D frustrated lattices, where the ESR linewidth was found constant for $T \gtrsim \theta$ [29,30].

We find the fits of the experimental linewidth [Fig. 2(c)] virtually indistinguishable for the SI and the DM model. At 500 K we extract $\sqrt{c}|D| = 0.53$ K, $a/D = 1.06$, $F/D = 0.09$ for the SI model and $\sqrt{c}|d_c| = 0.13$ K, $d_{ab}/d_c = 2.6$ for the DM model. It is worth noting that since Fe^{3+} is in the orbital S state, in the SI model only the a term is allowed in purely cubic, octahedral or tetrahedral environments. In BNFSO the local symmetry is lower; therefore, D and a can have similar magnitudes [24]. Although the absolute size or the sign of the anisotropy terms cannot be revealed from these fits due to unknown $c > 1$, the constant ratio $\Delta B_\perp / \Delta B_\parallel = 1.27$, observed in BNFSO above $\sim\theta$ [inset in Fig. 2(b)], unambiguously sets the ratio of the anisotropy terms for both models [25]. The temperature-independent linewidth ratio reveals that correlations are isotropic in spin space.

In our attempt to determine and quantify the dominant magnetic anisotropy in BNFSO, we now turn to high-frequency measurements. In contrast to the X band, we can follow the ESR signal across T_N [Fig. 3(a)]. The resonance broadens and shifts to lower field by ~ 2 T below T_N. The temperature dependence of the line shift mimics an order parameter [Fig. 3(b)], and corresponds to the opening of a zero-field gap in magnetic excitations (Fig. 4). This transformation of the paramagnetic signal into a collective antiferromagnetic resonance (AFMR)

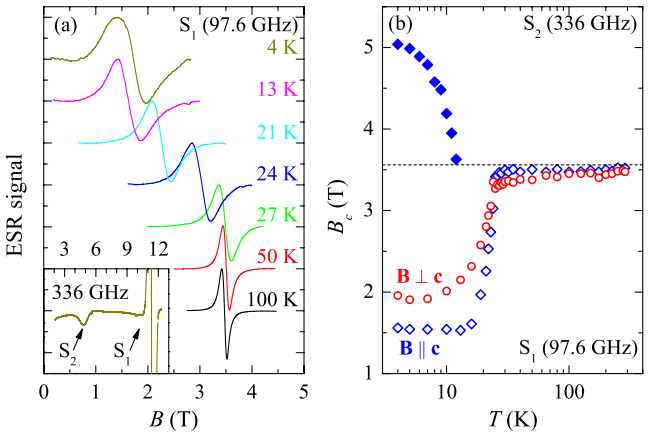

FIG. 3 (color online). (a) Selected ESR spectra at 97.6 GHz. Inset shows two distinct resonance modes at 4 K. (b) Temperature dependence of the central field of the two observed modes.

mode S_1 is accompanied by emergence of another AFMR mode (S_2) in our frequency window [inset in Fig. 3(a)]. The frequency-field diagram of the two modes is shown in Fig. 4 for both relevant directions of the applied field with respect to the crystallographic c axis.

We have simulated the AFMR modes experimentally detected at 4 K in a mean-field approximation [25], again for both types of magnetic anisotropy [Figs. 4(a) and 4(b)]. We note that the zero-field gap to the lowest gapped branch

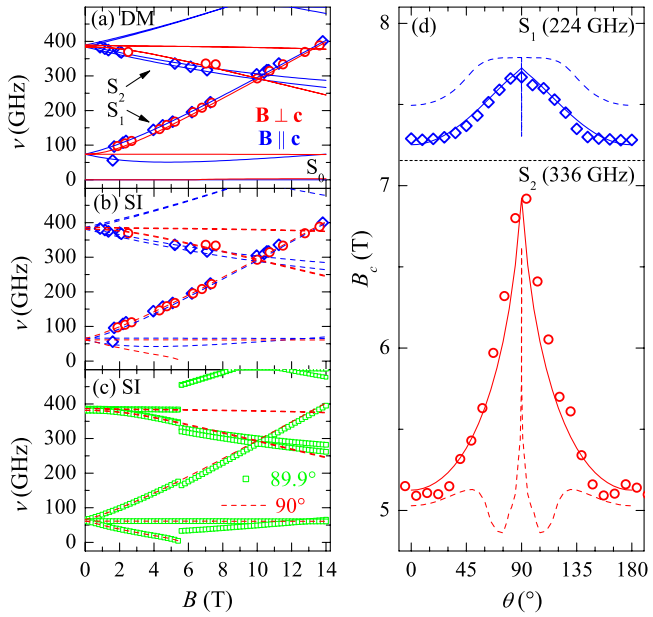

FIG. 4 (color online). Frequency-field diagram of measured (symbols) and simulated (lines) AFMR modes for (a) DM and (b) SI anisotropy at 4 K. (c) Field-induced phase transition predicted by the SI anisotropy model at 5.5 T for $\mathbf{B} \perp \mathbf{c}$. (d) Angular dependence of the two resonance modes at 4 K; measured (symbols) and simulated for the DM (solid lines) and SI anisotropy (dashed lines).

S_1 is opened by finite anisotropy (d_c or D, a, F) in a square-root fashion [25], while the gap to the next branch S_2 is present already for isotropic $\mathcal{H}_e$ and only slightly shifts with anisotropy. The latter gap is reproduced with the exchange parameters $J_1 = 11.9$ K, $J_2 = 3.4$ K, $J_3 = 0.72$ K, $J_4 = 0.24$ K, and $J_5 = 3.4$ K, which corresponds to a 20% increase [31] of the parameters obtained in the INS study [18].

The SI model [Eq. (2)], at first sight, yields a reasonable description of the experimental $\nu - B$ diagram [Fig. 4(b)] for $D = -17$ mK, $a = -18$ mK, and $F = -0.9$ mK [32]. However, a closer look at this model unveils its inconsistencies with the experiment. The simulated angular dependence of the two AFMR modes does not match the experiment [Fig. 4(d)]. The predicted nonmonotonic dependence of the S_2 mode is a consequence of a field-induced phase transition, occurring around 5.5 T [33] for $50° < \theta < 90°$ [see the discontinuity of curves in Fig. 4(c)]. The apparent absence of the transition at exactly $\theta = 90°$ is accidental, which can be deduced from Fig. 4(c). The transition corresponds to the field where the lowest branch reaches zero frequency. Such behavior was indeed observed and justified with the SI model on another Fe-based triangular lattice [34]. The absence of any irregularities in low-temperature magnetization isotherms speaks against such transition in BNFSO at least up to 23 T [35]. We stress that, on the other hand, no such excitation softening exists for the DM model [Fig. 4(a)]. Finally, the SI model predicts the selection of the $(\epsilon_H, \epsilon_\Delta) = (-1, 1)$ GS independent of the structural chirality. This contradicts with the experimental observation of the $(1, -1)$ GS in a crystal with structural left handedness [18], clearly making the SI model incompetent of selecting the proper ground state. This selection is independent of the structural chirality, because it is a single-ion property.

The DM model [Eq. (3)], on the other hand, yields excellent agreement with the experiment for $|d_c| = 45$ mK. Both the $\nu - B$ diagram [Fig. 4(a)] and the finer-detail angular dependence of both AFMR modes [Fig. 4(d)] are simulated convincingly. The DM anisotropy d_c explains the ESR linewidth and the finite gap to the S_1 branch. Its relative size $|d_c/J_1| = 0.4\%$ is in good agreement with the order-of-magnitude prediction $\Delta g/g = 0.25\%$, as derived by Moriya [5]. We note that the zero-field gap could also be explained by the presence of symmetric anisotropic exchange (AE) of a similar size $|J^{\mathrm{AE}}/J_1| = 0.4$–$0.8\%$ [25]. However, as the AE anisotropy results from the second order perturbation in λ (while DM anisotropy results from the first order perturbation), it is of the size [5] $(\Delta g/g)^2 J_1 = 6 \times 10^{-6} J_1$ and therefore negligible. We stress that the in-plane DM component d_{ab} does not affect the detected lowest branches and cannot be determined from the studies of these excitations. This makes the above-presented X-band ESR investigation, yielding $d_{ab}/d_c = 2.6$, invaluable in determining also the $|d_{ab}| = 120$ mK DM component. There is a very good agreement between the excitations observed in ESR and calculated with the DM model on one hand and the modes identified from the INS experiments [22,36] on the other hand. The calculated S_0 branch [Fig. 4(a)] is the gapless Goldstone mode emerging at the origin of the reciprocal space (scattering vector $Q = 0$) for the correlations of the c-axis spin components. The S_1 mode corresponds to the other, gapped excitations for chiral correlations of the ab-plane spin components at $Q = 0$. These excitations at $Q = \pm\mathbf{q}$ involve correlations of the c-axis spin-component [22] and cross $Q = 0$ at ≈ 400 GHz, yielding the S_2 signal.

The DM anisotropy thus proves to be the origin of the unique magnetic properties of BNFSO. Our simulations [25] further disclose that one of the two possible GSs [Fig. 1(b)] is selected depending on the sign of d_c. The experimentally detected GS $(1, -1)$ is realized for $d_c > 0$, when the DM energy [Eq. (3)] is minimized. Formation of a uniform vector chiral state at finite temperature is, however, challenged by formation of domain walls, which prosper on frustrated lattices due to thermal fluctuations [37]. It is likely that these are responsible for diffuse neutron scattering coexisting with the LRO state in BNFSO far below T_N [38]. It is therefore striking that the minute $d_c = 45$ mK term effectively imposes a single-domain GS at 2 orders of magnitude larger temperatures, as experimentally verified at 1.5 K [18], and a chiral unbalance up to T_N, with chiral correlations persisting even in the paramagnetic state [23].

In conclusion, we have shown that the selection of the unique chiral magnetic ground state in BNFSO is due to the Dzyaloshinsky-Moriya interaction as the dominant source of magnetic anisotropy. Although this term is small ($d_c = 45$ mK, $d_{ab} = 120$ mK), it effectively overcomes thermal fluctuations and leads to a fully chiral state in structurally enantiopure crystals, whereas spin-liquid signatures might also be anticipated above T_N, possibly with Skyrmion texturation [39,40].

We thank S. de Brion for fruitful discussion and acknowledge the financial support of the Slovenian Research Agency (Projects No. J1-2118 and No. BI-US/09-12-040).

[1] *Introduction to Frustrated Magnetism*, edited by C. Lacroix, P. Mendels, and F. Mila (Springer-Verlag, Berlin, 2011).
[2] L. Balents, Nature (London) **464**, 199 (2010).
[3] S. T. Bramwell and M. J. P. Gingras, Science **294**, 1495 (2001).
[4] A. Zorko *et al.*, Phys. Rev. Lett. **107**, 047208 (2011).
[5] T. Moriya, Phys. Rev. **120**, 91 (1960).
[6] M. Elhajal, B. Canals, and C. Lacroix, Phys. Rev. B **66**, 014422 (2002).
[7] R. Ballou *et al.*, J. Magn. Magn. Mater. **262**, 465 (2003).

[8] K. Matan *et al.*, Phys. Rev. Lett. **96**, 247201 (2006).
[9] O. Cépas *et al.*, Phys. Rev. B **78**, 140405 (2008).
[10] K. Penc *et al.*, Phys. Rev. Lett. **99**, 117201 (2007).
[11] O. A. Starykh, H. Katsura, and L. Balents, Phys. Rev. B **82**, 014421 (2010).
[12] P. Bak and M. H. Jensen, J. Phys. C **13**, L881 (1980).
[13] D. Grohol *et al.*, Nature Mater. **4**, 323 (2005).
[14] Y. Machida *et al.*, Nature (London) **463**, 210 (2009).
[15] M. Mostovoy, Phys. Rev. Lett. **96**, 067601 (2006).
[16] Y. Taguchi *et al.*, Science **291**, 2573 (2001).
[17] X. G. Wen, F. Wilczek, and A. Zee, Phys. Rev. B **39**, 11 413 (1989).
[18] K. Marty *et al.*, Phys. Rev. Lett. **101**, 247201 (2008).
[19] K. Marty *et al.*, Phys. Rev. B **81**, 054416 (2010).
[20] H. D. Zhou *et al.*, Chem. Mater. **21**, 156 (2009).
[21] C. Lee *et al.*, Chem. Mater. **22**, 5290 (2010).
[22] M. Loire *et al.*, Phys. Rev. Lett. **106**, 207201 (2011).
[23] C. Stock *et al.*, Phys. Rev. B **83**, 104426 (2011).
[24] A. Abragam and B. Bleaney, *Electron Paramagnetic Resonance of Transition Ions* (Clarendon, Oxford, 1970).
[25] See Supplemental Material at http://link.aps.org/supplemental/10.1103/PhysRevLett.107.257203 for details on the *X*-band ESR *g*-factor and linewidth fitting as well as for modeling of the AFMR modes at higher frequencies.
[26] Dipolar interaction between Fe^{3+} moments and their hyperfine coupling to nuclear moments are negligible—they yield linewidths of $\Delta B \lesssim 3$ mT due to strong exchange narrowing. Symmetric anisotropic exchange being a quadratic correction in λ is inferior to the antisymmetric Dzyaloshinsky-Moriya term being linear in λ [5].
[27] A. Bencini and D. Gatteshi, *EPR of Exchange Coupled Systems* (Springer-Verlag, Berlin, 1990).
[28] R. Kubo and K. Tomita, J. Phys. Soc. Jpn. **9**, 888 (1954).
[29] A. Zorko *et al.*, Phys. Rev. B **69**, 174420 (2004).
[30] A. Zorko *et al.*, Phys. Rev. Lett. **101**, 026405 (2008).
[31] The increase of the exchange parameters by 20% compared to those from the INS experiment [18] is necessary because we use the experimental value of the ordered moments 4 μ_B instead of the full value 5 μ_B.
[32] Other selections of the sign for the SI parameters do not yield AFMR modes resembling the experiment.
[33] The critical field is shifted to 7.5 T if exchange parameters from Ref. [23], which are significantly different, are used.
[34] A. I. Smirnov *et al.*, Phys. Rev. B **75**, 134412 (2007).
[35] K. Marty, Ph.D. thesis, University of Grenoble, 2008; http://tel.archives-ouvertes.fr/tel-00351575/en/.
[36] J. Jensen, Phys. Rev. B **84**, 104405 (2011).
[37] J. T. Chalker, P. C. W. Holdsworth, and E. F. Shender, Phys. Rev. Lett. **68**, 855 (1992).
[38] H. D. Zhou *et al.*, Phys. Rev. B **82**, 132408 (2010).
[39] C. Pappas *et al.*, Phys. Rev. Lett. **102**, 197202 (2009).
[40] C. Pappas *et al.*, Phys. Rev. B **83**, 224405 (2011).